SIAM J. APPL. MATH.
Vol. 69, No. 2, pp. 473–493

OSTWALD RIPENING IN THIN FILM EQUATIONS*

K. B. GLASNER†

Abstract. Fourth order thin film equations can have late stage dynamics that are analogous to the classical Cahn–Hilliard equation. We undertake a systematic asymptotic analysis of a class of equations that describe partial wetting with a stable precursor film introduced by intermolecular interactions. The limit of small precursor film thickness is considered, leading to explicit expressions for the late stage dynamics of droplets. Our main finding is that exchange of mass between droplets characteristic of traditional Ostwald ripening is a subdominant effect over a wide range of kinetic exponents. Instead, droplets migrate in response to variations of the precursor film. Timescales for these processes are computed using an effective medium approximation to the reduced free boundary problem, and dynamic scaling in the reduced system is demonstrated.

Key words. thin film equation, dewetting, coarsening, Ostwald ripening

AMS subject classifications. 76D08, 34E05

DOI. 10.1137/080713732

1. Introduction.

Viscous liquid films have a rich set of dynamics that are still only partially understood [7, 28]. A large subset of phenomena involves dewetting instabilities that produce a diverse collection of patterns that have been studied experimentally [1, 13, 33, 34, 35, 42] as well as theoretically [2, 3, 19, 22, 27, 36, 37, 42]. These instabilities cause nearly uniform fluid layers to break up into arrays of large droplets connected by a remaining (very) thin film, which undergo an elaborate coarsening process characterized both by coalescence of droplets and exchange of fluid between droplets and the intervening film [11, 12, 15, 16].

The results we describe run parallel to other studies of dynamical coarsening processes, most notably phase separation phenomena described by the Cahn–Hilliard equation [5, 30]. At late times and small volume fractions, this equation describes the Ostwald ripening process [14, 24, 25, 38, 39]. Our purpose is to describe a similar limit for a class of thin film equations and to highlight the differences between our problem and classical Ostwald ripening.

The analogy between spinodal decomposition and liquid dewetting was first explored by Mitlin [19, 20, 21, 22]. Subsequent theoretical works have studied coarsening in thin film equations that results from other instabilities. Bestehorn, Pototsky, and Thiele [4] consider the evolution of a film destabilized by Marangoni effects and quantify coarsening rates through numerical experiments. Merkt et al. [18] obtain similar results for a two-layer film. There are, in fact, numerous other variations of dissipative fourth order equations that exhibit coarsening behavior, for example, the convective Cahn–Hilliard equation studied by Watson et al. [40].

This paper is a continuation of a body of work initiated by Glasner and Witelski [11, 12] on coarsening behavior of liquid droplets described by disjoining-pressure models. It was found there that the dewetting instability leads to the eventual development of droplets separated by a precursor film. The subsequent one-dimensional

*Received by the editors January 18, 2008; accepted for publication (in revised form) July 18, 2008; published electronically November 14, 2008. This work was produced with the assistance of NSF award DMS-0405596.

http://www.siam.org/journals/siap/69-2/71373.html

†Department of Mathematics, University of Arizona, 617 N. Santa Rita, Tucson, AZ 85721 (kglasner@math.arizona.edu).

dynamics of these droplets was computed, involving mass exchange between droplets and the precursor layer as well as motion of the droplets themselves. This results in a coarsening process characterized by both mass transfer and coalescence, and exhibits dynamic scaling with a nonstandard exponent. Rigorous bounds for dynamic scaling were subsequently obtained by Otto, Rump, and Slepčev [29]. In two dimensions, the interaction of droplets has been studied by Pismen and Pomeau [32]. Although not entirely dissimilar from the conclusions described here, their results are in both quantitative and qualitative disagreement with our calculations (see the concluding section for a comparison).

This work serves as a companion paper to the manuscript of Glasner et al. [9]. Instead of a matched asymptotics approach, that work utilizes a variational principle (the Rayleigh–Onsager notion of least dissipation [26]) to explain and quantify droplet migration effects. Both papers obtain comparable results, although a careful interpretation is needed to show their equivalence. Some comparison is provided in section 5.

This paper considers a class of fourth order parabolic equations which have the structure

$$\tau(\epsilon)h_t = \nabla\cdot(h^q\nabla p), \qquad p = \epsilon^{-1}U'\left(\frac{h}{\epsilon}\right) - \Delta h, \quad q > 0. \tag{1.1}$$

The physical domain is taken to be a two-dimensional, bounded, simply connected open set Ω, where Neumann and no-flux boundary conditions are imposed (although few of our results depend crucially on these assumptions). The timescale $\tau(\epsilon)$ is chosen to capture the slow dynamics associated with migration and mass exchange (i.e., ripening) of droplets. It depends on the mobility exponent as

$$\tau(\epsilon) = \begin{cases} \epsilon^q, & q \in (0,2), \\ \epsilon^2 \ln(\epsilon^{-1}), & q = 2, \\ \epsilon^2, & q \in (2,3), \\ \epsilon^2/\ln(\epsilon^{-1}), & q = 3, \\ \epsilon^{q-1}, & q > 3. \end{cases} \tag{1.2}$$

Our interest is in the limit of small ϵ, which corresponds to both thin precursor films and long timescales.

It is instructive to consider a range of mobility exponents to capture the crossover between different dynamical mechanisms. For liquid films, this exponent is a function of the solid-liquid boundary condition and the fluid rheology. The standard case of a Newtonian fluid with a no-slip boundary condition corresponds to $q = 3$. The Navier slip condition leads to $q = 2$ if particular limits are considered [8, 23], whereas Darcy's law can lead to $q = 1$ [6]. Models of non-Newtonian fluids may have a variety of exponents (see, e.g., [41]).

The class of potentials U considered here include those commonly employed to describe a combination of attractive and repulsive van der Waals forces [28]. The following assumptions are used:

1. U is scaled so that it has a minimum at 1 and $U(\infty) - U(1) = 2$.
2. U' has a unique maximum at $H^* > 1$.
3. The potential decays as

$$U'(H) = \mathcal{O}(H^{-\alpha}), \quad H \to \infty, \tag{1.3}$$

where

$$\alpha > \begin{cases} q+1, & q \in (0,2), \\ 3, & q \geq 2. \end{cases} \tag{1.4}$$

This will ensure that intermolecular interactions have a subdominant effect for macroscopic ($h \sim \mathcal{O}(1)$) films.

The structure of the paper is as follows. Section 2 describes the results of the lengthy calculation, whose details are given in sections 3 and 4. Section 5 goes on to propose an approximation procedure for the resulting free boundary problem, and timescales for the relevant dynamics are worked out. Section 6 gives example calculations and compares them to predictions of dynamic scaling.

2. Setup for matched asymptotics and a summary of results. There will be three regions in the matched asymptotic analysis (see Figure 2.1):

- Region I: This region corresponds to droplets and is composed of the union of disjoint disks $\{D_i\}$ which have the form $D = \{\mathbf{x} \mid |\mathbf{x} - X| < R\}$ so that X is the droplet center and R is its radius. Unit normals to ∂D will be denoted $\mathbf{n}$, and we will also utilize the coordinate unit vectors $\hat{\mathbf{x}}$, $\hat{\mathbf{y}}$, etc. In this region, h and x will both scale like $\mathcal{O}(1)$. It will be convenient to use the moving polar coordinates $r = |\mathbf{x} - X(t)|$, $\theta = \arg(\mathbf{x} - X(t))$.
  To be more precise about R and X, we define the contact line at finite ϵ to be the set $\{\mathbf{x} \mid h(\mathbf{x}) = \epsilon H^*\}$, where H^* is the global maximum of U'. This definition is somewhat arbitrary and is chosen merely for convenience. On the other hand, in the limit $\epsilon \to 0$ this set converges to the boundary of the support of h, i.e., the sharp-interface contact line. We suppose that for each droplet this curve is nearly circular and has the form $\mathbf{x} = X + R(\theta)\hat{\mathbf{r}}$. Properly speaking, R and X should also be expanded in ϵ, but to avoid

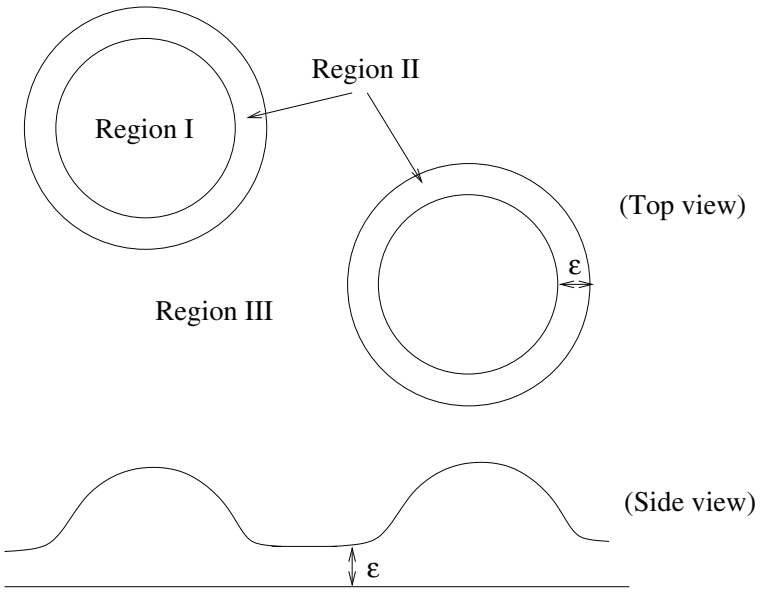

FIG. 2.1. *Three regions for the matched asymptotic calculation.*

excessive notation, these labels will simply denote the corresponding leading order solutions. In particular, we find that R is independent of θ at leading order.

- Region II is a microscopic internal layer near the contact line where h and x scale like ϵ. The moving rescaled radial coordinate

$$z = \frac{R(t) - r}{\epsilon} \tag{2.1}$$

will be employed. In light of the definition of R, the solution in this region must satisfy

$$h(z = 0) = h^*. \tag{2.2}$$

For reference, the Laplacian in z, θ coordinates expands as

$$\Delta h = \epsilon^{-2} h_{zz} - \epsilon^{-1} R^{-1} h_z - \left(z R^{-2} h_z + R^{-2} h_{\theta\theta} \right) + \mathcal{O}(\epsilon). \tag{2.3}$$

- Region III is the complement $\Omega / \cup D_i$ which contains the precursor film. In this region, h will scale like ϵ.

The overall strategy is to propose self-consistent asymptotic expansions in each region and to connect them via matching conditions. Less-standard matching conditions are derived when needed. Corrections to the leading order base solutions solve linear equations, and Fredholm-type solvability conditions will yield information about the dynamics.

The main goal is to determine the dynamic behavior of R and X, which will be shown to arise from a flux J which is determined by the elliptic problem

$$\Delta P = 0, \quad P|_{\partial D_i} = \frac{2}{R_i}, \quad J = -\nabla P, \tag{2.4}$$

solved in the exterior region $\Omega / \cup D_i$. Here P represents the first nontrivial correction to the pressure p. Equations (2.4) describe quasi-steady diffusion of material driven by a Gibbs–Thomson boundary condition. We find that, with respect to the timescale τ, the dynamics at leading order are

$$R_t = \begin{cases} -\frac{4}{3\pi R^2} \int_{\partial D} J \cdot \mathbf{n} \, ds, & q < 2, \\ 0, & q \geq 2, \end{cases} \tag{2.5}$$

and

$$X_t = -M(R) \int_{\partial D} \mathbf{n} J \cdot \mathbf{n} \, ds, \tag{2.6}$$

where the mobility factor $M(R)$ is

$$M = \frac{1}{\pi} \begin{cases} R^{-2} \Psi_1(1) \Big/ \int_0^1 \Psi_1(r) r^2 dr, & q < 2, \\ R^{-2} \Big/ \int_0^1 \Psi_1(r) r^2 dr, & q = 2, \\ R^{q-4} \int_{-\infty}^{\infty} [H_1^{1-q} - H_1^{-q}] dz \Big/ \int_0^1 \Psi_1(r) r^2 dr, & q \in (2, 3), \\ R^{-1} \int_{-\infty}^{\infty} [H_1^{-2} - H_1^{-3}] dz, & q = 3, \\ R^{-1} \int_{-\infty}^{\infty} [H_1^{1-q} - H_1^{-q}] dz \Big/ \int_{-\infty}^{\infty} H_1^{2-q} - H_1^{1-q} dz, & q > 3. \end{cases} \tag{2.7}$$

H_1 is the leading order solution for the microscopic contact line region II. The function Ψ_1 arises from the solvability argument and is specified as the solution of the rescaled boundary value problem (4.5)–(4.7).

The point of writing $R_t = 0$ for $q \geq 2$ in (2.5) is to emphasize the crossover between radial and migration dynamics. This is to some extent an artifact of our choice of timescales (1.2). Had we chosen $\tau = \epsilon^q$ for all q instead, then the radial dynamics would just be given by the first nonzero formula in (2.5).

3. Base solutions. This section summarizes the aspects of the analysis which are common to all mobility exponents $q > 0$. The rest is split into cases in the following section.

Region II. The solution is expanded as $h = \epsilon H_1 + \epsilon^2 H_2 + o(\epsilon^2)$. The leading order equation is

$$(H_1^q[-(H_1)_{zz} + U'(H_1)]_z)_z = 0. \tag{3.1}$$

Integrating twice and using the matching conditions $(H_1)_z \sim 0$ as $z \to -\infty$, we get

$$-(H_1)_{zz} + U'(H_0) = c_1. \tag{3.2}$$

The matching condition $(H_1)_{zz} \sim 0$ as $z \to +\infty$ means that $C = 0$ in light of (1.3). It follows that $H_1 \sim 1$ as $z \to -\infty$, and we can integrate again to obtain

$$\frac{1}{2}(H_1)_z^2 = U(H_1) - U(1), \tag{3.3}$$

from which the equilibrium contact angle is determined by

$$(H_1)_z = \sqrt{2[U(H_1) - U(1)]} \sim 1, \quad z \to +\infty. \tag{3.4}$$

Solving (3.3) gives the solution implicitly as

$$\int^{H_1} \frac{dH}{\sqrt{2[U(H) - U(1)]}} = z + c_2. \tag{3.5}$$

The constant of integration is determined uniquely by the condition (2.2).

The next order correction satisfies

$$(H_1^q[-(H_2)_{zz} - R^{-1}(H_1)_z + U''(H_1)H_2]_z)_z = 0. \tag{3.6}$$

Integrating and using the matching condition $(H_2)_{zzz} \to 0$ as $z \to \infty$ gives

$$[-(H_2)_{zz} - R^{-1}(H_1)_z + U''(H_1)H_2]_z = 0. \tag{3.7}$$

A further integration implies

$$-(H_2)_{zz} - R^{-1}(H_1)_z + U''(H_1)H_2 \equiv P = \text{constant}. \tag{3.8}$$

This says that (total) leading order pressure is constant through region II, and we can use this to match between regions I and III. We remark that both H_1 and H_2 are independent of θ. Later in the calculation, this will provide symmetry that is needed to make certain integrals vanish.

Region I. Expanding $h = h_0(\mathbf{x}, t) + o(1)$ for now, we obtain

$$\nabla\cdot(h_0^q \nabla \Delta h_0) = 0, \quad \mathbf{x} \in D. \tag{3.9}$$

Provided that h_0 is well behaved (bounded third derivatives), integration of (3.9) against Δh_0 gives

$$\int_D h_0^q |\nabla \Delta h_0|^2 dx = 0. \tag{3.10}$$

Since $h_0 \to 0$ on the boundary of D, it follows that Δh_0 is a constant. Using the matching conditions

$$h_0(R,\theta) = 0, \quad (h_0)_r(R,\theta) = -1 \tag{3.11}$$

gives the family of radially symmetric droplet solutions

$$h_0(\mathbf{x}; R(t), X(t)) = R(t) H\left(\frac{\mathbf{x} - X(t)}{R(t)}\right), \quad H(\eta) = \frac{1}{2}(1-\eta^2). \tag{3.12}$$

Using (3.8), (3.12) and the matching condition

$$(h_0)_{rr}(R,\theta) = \lim_{z\to\infty} (H_2)_{zz} \tag{3.13}$$

allows us to relate the pressure P and the droplet radius:

$$P = -\Delta h_0 = \frac{2}{R(t)}. \tag{3.14}$$

Region III. Here we expand $h = \epsilon h_1 + \epsilon^2 h_2 + o(\epsilon^2)$. Because of the scaling of $\tau(\epsilon)$, the leading order problem for all $q > 0$ is the elliptic equation

$$\nabla\cdot(h_1^q \nabla U'(h_1)) = 0. \tag{3.15}$$

Matching to region II implies $h_1 = 1$ on the boundary $\cup \partial D_i$; therefore $h_1 \equiv 1$. At order ϵ^2, the correction term satisfies the "quasi-steady" problem

$$\Delta h_2 = 0. \tag{3.16}$$

This equation is solved together with boundary conditions that are derived by matching. Using (3.8) and (3.14), we find that

$$U''(1) h_2 = \frac{2}{R(t)}, \quad \mathbf{x} \in \partial D. \tag{3.17}$$

It is convenient introduce the flux

$$J = -h^q \nabla p = -\epsilon^q U''(1) \nabla h_2 + o(\epsilon^q) \tag{3.18}$$

so that at leading order

$$J_q = -\nabla P, \quad P \equiv U''(1) \nabla h_2 \tag{3.19}$$

is therefore determined by solving the boundary value problem (3.16), (3.17). To avoid excessive notation, we also use J_q to denote the flux of order $\mathcal{O}(\epsilon^q)$ in regions I and II.

4. Mobility-dependent expansions.

4.1. Case $q \in (0,2)$. The expansion of the equation in region II at order ϵ^q gives $0 = (J_q \cdot \hat{\mathbf{z}})_z$, which merely says that the z-component of J_q is constant through this layer. Thus the normal component of J_q to the boundary of D is that given by the solution in region III.

In region I, we expand $h = h_0(x,t) + \epsilon^q h_q + o(\epsilon^q)$, which means that leading order flux is $J_q = h_0^q \nabla \Delta h_q$. The first nontrivial correction to the equation in this region gives the linear problem

$$\mathcal{L} h_q = X_t \cdot \nabla h_0 - R_t \frac{\partial h_0}{\partial R}, \quad \mathcal{L} = \nabla \cdot [h_0^q \nabla \Delta \tag{4.1}$$

for $\mathbf{x} \in D$ (the mismatched bracket indicates that the divergence applies to everything to the right). We remark that a similar linear problem was encountered by Pismen [31]. The linear operator $\mathcal{L}$ (on a space endowed with suitable homogeneous boundary conditions) has the adjoint

$$\mathcal{L}^\dagger = \Delta \nabla \cdot [h_0^q \nabla . \tag{4.2}$$

Nullspace of $\mathcal{L}^\dagger$. To invoke a Fredholm solvability argument, we need to characterize its nullspace by finding orthogonal functions whose span is the same as $\{(h_0)_x, (h_0)_y, (h_0)_R\}$. Observe that if ψ is in the nullspace, then

$$\nabla \cdot \left[h_0^q \nabla \psi \right] = \phi, \quad \Delta \phi = 0. \tag{4.3}$$

We shall be interested in the particular harmonic functions $\phi = 0, -x, -y$, which ultimately correspond to changes in droplet size and translation in each direction, respectively. Since $x = r\cos\theta$, $y = r\sin\theta$, we look for a solution of (4.3a) of the form $\psi = \Psi(r)\cos\theta$ or $\psi = \Psi(r)\sin\theta$. In either case we are led to the differential equation

$$r(r h_0^q \Psi')' - h_0^q \Psi = -r^3 \tag{4.4}$$

together with the boundary conditions

$$h_0^q \Psi'(R) = 0, \quad \Psi(0) = 0. \tag{4.5}$$

Several observations about (4.4)–(4.5) are in order. First, the solution is unique, since multiplying the homogeneous version of this linear equation by Ψ/r and integrating leads to

$$\int_0^R \left[r h_0^q \Psi'^2 + \frac{h_0^q \Psi^2}{r} \right] dr = 0. \tag{4.6}$$

There is also a natural scale invariance for this problem: If Ψ_1 solves

$$r(r H^q \Psi_1')' - H^q \Psi_1 = r^3, \quad \Psi_1(0) = 0, \quad H^q \Psi_1(1) = 0, \tag{4.7}$$

then

$$\Psi = R^{3-q} \Psi_1(r/R) \tag{4.8}$$

solves (4.4). Finally, the regularity of solutions of the ordinary differential equation (4.4) and the first boundary condition (4.5) allow us to ascertain the asymptotics at

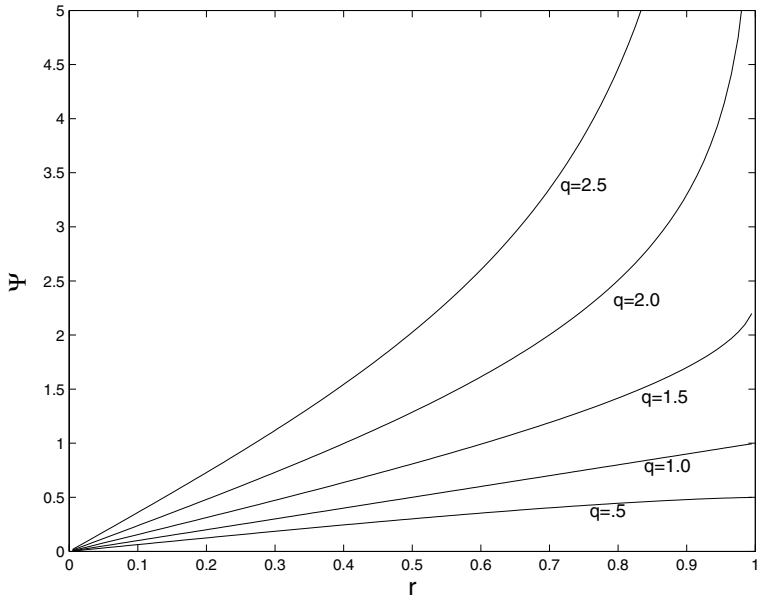

FIG. 4.1. *The function $\Psi(r)$ with $R = 1$, used in the solvability argument.*

$r = R$. In particular, we have $h_0^q \Psi'(R) = \mathcal{O}(|r - R|)$, and therefore one computes for $r \to R$

$$\Psi \sim \begin{cases} \mathcal{O}(1), & q < 2, \\ R \ln |r - R|, & q = 2, \\ \frac{R}{q-2} |r - R|^{2-q}, & q > 2. \end{cases} \tag{4.9}$$

In particular, Ψ is bounded for $q < 2$ and integrable for $q < 3$. Since $r = R$ is a regular singular point of (4.4), the first boundary condition in (4.5) implies

$$h_0^q \Psi'(r) = \mathcal{O}(|r - R|), \quad r \to R. \tag{4.10}$$

In practice, solutions to (4.4) can be obtained numerically (see Figure 4.1). To summarize, the desired functions for the solvability argument are

$$\psi_R = 1, \quad \psi_x = \Psi(r) \cos\theta, \quad \psi_y = \Psi(r) \sin\theta. \tag{4.11}$$

Solvability conditions. The inner product of ψ_R with (4.1) produces

$$R_t = -\frac{\int_{\partial D} h_0^q \nabla \Delta h_q \cdot \mathbf{n} \, ds}{\int_D \partial h_0 / \partial R \, dx}. \tag{4.12}$$

Using the matching condition for flux,

$$R_t = -\frac{4}{3\pi R^2} \int_{\partial D} J_q \cdot \mathbf{n} \, ds. \tag{4.13}$$

This is just a statement about conservation of the droplet volume $V = \int h_0 \, dx = \pi R^3/4$ since

$$V_t = -\int_{\partial D} J_q \cdot \mathbf{n} \, ds. \tag{4.14}$$

Inner products of (4.1) with $\psi_{x,y}$ determine the translation dynamics. Integration with ψ_x gives

$$\begin{aligned} X_t \cdot \hat{\mathbf{x}} \int_D \psi_x \frac{\partial h_0}{\partial x} d\mathbf{x} &= \int_{\partial D} \psi_x h_0^q \nabla \Delta h_q \cdot \mathbf{n}\, ds - \int_{\partial D} h_0^q (\Delta h_q) \nabla \psi_x \cdot \mathbf{n} ds \\ &\quad - \int_{\partial D} x \nabla h_q \cdot \mathbf{n} ds + \int_{\partial D} h_q \cos\theta\, ds \\ &\equiv \int_{\partial D} \psi_x J_q \cdot \mathbf{n}\, ds + B_1 + B_2 + B_3. \end{aligned} \tag{4.15}$$

In writing this, the inner products with $\partial h_0/\partial y$ and $\partial h_0/\partial R$ are zero by symmetry. We will argue that $B_1 = B_2 = B_3 = 0$.

First, since the leading order flux is constant across region II,

$$J_q \cdot \mathbf{n} = h_0^q \nabla \Delta h_q \cdot \mathbf{n} = \mathcal{O}(1), \quad r \to R. \tag{4.16}$$

Therefore

$$\nabla \Delta h_q \cdot \mathbf{n} = \mathcal{O}(|r-R|)^{-q}, \quad \Delta h_q = \mathcal{O}(|r-R|^{-q+1}), \quad r \to R. \tag{4.17}$$

Using (4.10), this means that

$$h_0^q (\psi_x)_z \Delta h_q = \mathcal{O}(|r-R|^{-q+2}), \quad r \to R, \tag{4.18}$$

so that integral $B_1 = 0$.

For the integrals B_2 and B_3, consider first the subcase $q = 1$. The relevant matching conditions are

$$h_1(R,\theta) = \lim_{z\to\infty} H_1(z), \quad (h_1)_r(R,\theta) = \lim_{z\to\infty} H_2'(z). \tag{4.19}$$

Since H_1 and H_2 are independent of θ, the integrals B_2 and B_3 vanish by symmetry.

For noninteger q, the terms in the region II expansion necessary for matching would be orders ϵ^q and ϵ^{q+1}. If such orders were included in the expansion, they would solve equations like

$$\left(H_1^q [(H_n)_{zz} - U''(H_1) H_n]_z \right)_z = 0, \tag{4.20}$$

where $1 < n < 3$. Since there is no flux of order $\epsilon^{q+n-3} > \epsilon^q$, integrating (4.20), one gets

$$(H_n)_{zz} - U''(H_1) H_n = \text{constant}. \tag{4.21}$$

From this it is seen that the solution H_n of *any* order $n < 3$ is independent of θ, and therefore the integrals B_2 and B_3 again vanish.

We now return to determining the migration dynamics. A similar argument as presented holds for the inner product with ψ_y. Using (4.11), (4.15) and $\mathbf{n} = (\cos\theta, \sin\theta)$ leads to

$$X_t = -\frac{1}{\pi} \frac{R\Psi(R)}{\int_0^R \Psi(r) r^2 dr} \left(\int_{\partial D} \mathbf{n} J_q \cdot \mathbf{n}\, ds \right). \tag{4.22}$$

Equations (4.13), (4.22) specify the droplet dynamics once the boundary value problem (3.16)–(3.18) is solved.

4.2. Case $q \in (2,3)$. As for the case of $p \leq 2$, in region II the flux of order ϵ^q involves the correction to H of order ϵ^3, which satisfies the linear equation

$$0 = (J_q \cdot \hat{\mathbf{z}})_z = \left(H_1^q \left[(H_3)_{zz} - R^{-1}(H_2)_z - zR^{-2}(H_1)_z + \frac{1}{2}U'''(H_1)H_2^2 + U''(H_1)H_3 \right]_z \right)_z. \tag{4.23}$$

The relevant solvability condition for the linear equation (4.23) is found by using the bounded function

$$\Phi(z) = -\int_z^\infty \frac{H_1 - 1}{H_1^q} dz', \tag{4.24}$$

which is in the adjoint nullspace of the linear operator in (4.23) and corresponds to translation. Taking an inner product with (4.23) gives

(4.25)

$$0 = \left[(J_q \cdot \hat{\mathbf{z}})\, \Phi - (H_1 - 1)[(H_3)_{zz} - U''(H_1)H_3] + (H_1)_z(H_3)_z - (H_1)_{zz}(H_3) \right]_{-\infty}^{\infty} + Q,$$

$$Q = \int_{-\infty}^{\infty} (H_1 - 1) \left[R^{-1}(H_2)_z + zR^{-2}(H_1)_z + \frac{1}{2}U'''(H_1)H_2^2 \right]_z dz.$$

Here $(J_q \cdot \hat{\mathbf{z}}) = -(J_q \cdot \mathbf{n})$ is just the flux matched to the region III solution at $z = -\infty$. Note that the term Q inherits radial symmetry from H_1, H_2 and therefore should be inconsequential for migration dynamics.

Applying the far field and matching conditions

$$\Phi \sim 0, \quad (H_1)_z \sim 1, \quad (H_3)_z \sim +\frac{\partial^2 h_1}{\partial r^2}(R,\theta)z - \frac{\partial h_2}{\partial r}(R,\theta), \quad z \to \infty, \tag{4.26}$$

$$H_1 \sim 1, \quad z \to -\infty, \tag{4.27}$$

to (4.25) gives

$$\left(J_q \cdot \hat{\mathbf{z}}\right) \int_{-\infty}^{\infty} \frac{H_1 - 1}{H_1^q} dz' = \frac{\partial h_2}{\partial r}(R,\theta) - Q. \tag{4.28}$$

In region I, we expand $h = h_0(x,t) + \epsilon h_1 + \epsilon^2 h_2 + o(\epsilon^2)$ and obtain the same as (4.1), except that it applies to the correction at order ϵ^2 instead of order ϵ^q:

$$\mathcal{L}h_2 = X_t \cdot \nabla h_0 - R_t \frac{\partial h_0}{\partial R}, \quad \mathcal{L} = \nabla \cdot [h_0^q \nabla \Delta, \quad \mathbf{x} \in D. \tag{4.29}$$

Solvability conditions are obtained as in case $q < 2$. An inner product with ψ_R gives

$$R_t = -\frac{\int_{\partial D} h_0^q \nabla \Delta h_2 \cdot \mathbf{n}\, ds}{\int_D \partial h_0 / \partial R\, dx}. \tag{4.30}$$

Note that $h_0^q \nabla \Delta h_2$ would be the flux at order ϵ^2, but this is zero since the leading order flux scales like ϵ^q. This means that $R_t = 0$ on the timescale specified by $\tau(\epsilon)$. One could potentially obtain the slow dynamics for mass exchange by going further in the expansion, where a result like (4.13) should follow on a timescale ϵ^q instead of $\tau(\epsilon)$.

For exponents $q \geq 2$ the functions ψ_x, ψ_y are not bounded at $r = R$, but we can integrate over a smaller disk D_ρ of radius ρ and take $\rho \to R$. To avoid excessive notation, the integrals $\int_D, \int_{\partial D}$ which appear below should be interpreted as this limit. Integration with ψ_x yields

$$\begin{aligned} X_t \cdot \hat{\mathbf{x}} \int_D \psi_x (h_0)_x \, d\mathbf{x} &= \int_{\partial D} \psi_x h_0^q \nabla \Delta h_2 \cdot \mathbf{n} ds - \int_{\partial D} h_0^q (\Delta h_2) \nabla \psi_x \cdot \mathbf{n} ds \\ &\quad - \int_{\partial D} x \nabla h_2 \cdot \mathbf{n} ds + \int_{\partial D} h_2 \cos\theta \, ds \\ &\equiv B_1 + B_2 + B_3 + B_4. \end{aligned} \tag{4.31}$$

In contrast to $p < 2$, only the boundary term B_3 is not zero. In light of (4.9), one has the asymptotics

$$\psi_x = \mathcal{O}(|r-R|^{2-q}), \quad \nabla \psi_x \cdot \mathbf{n} = \mathcal{O}(|r-R|^{1-q}), \quad h_0^q = \mathcal{O}(|r-R|^q). \tag{4.32}$$

The boundedness of derivatives of h_2 then implies $B_1 = B_2 = 0$. For B_4, matching to region I implies $H_2 \sim \frac{1}{2}(h_0)_{rr}(R,\theta) z^2 - (h_1)_r(R,\theta) z + (h_2)(R,\theta)$ for large z. This means that h_2 is independent of θ, and symmetry gives $B_4 = 0$. It follows that

$$X_t \cdot \hat{\mathbf{x}} \int_D \psi_x (h_0)_x \, d\mathbf{x} = - \int_{\partial D} x \nabla h_2 \cdot \mathbf{n} ds. \tag{4.33}$$

A similar expression can be obtained using ϕ_y. Combining this with (4.28), the terms involving Q drop away by symmetry, leaving

$$X_t = -\frac{1}{\pi} \frac{R^2 \int_{-\infty}^{\infty} H_1^{1-q} - H_1^{-q} dz'}{\int_0^R \Psi(r) r^2 dr} \left(\int_{\partial D} \mathbf{n} J_q \cdot \mathbf{n} ds \right). \tag{4.34}$$

4.3. Case $q > 3$. The expansion in region II is now done as $H = \epsilon H_1 + \epsilon^2 H_2 + \epsilon^3 H^3 + \cdots$. At the level of the first nonzero flux J_q, we get the linear equation

$$\begin{aligned} -(X_t \cdot \mathbf{n})(H_1)_z = \Bigg(H_1^q \Bigg[&(H_3)_{zz} - R^{-1}(H_2)_z - z R^{-2} (H_1)_z \\ &+ \frac{1}{2} U'''(H_1) H_2^2 + U''(H_1) H_3 \Bigg]_z \Bigg)_z. \end{aligned} \tag{4.35}$$

The solvability argument proceeds as for the case $2 < q < 3$ and uses the bounded function Φ defined in (4.24). The inner product with (4.35) gives the same result as for $2 < q < 3$ except that the left-hand side is nonzero:

$$(X_t \cdot \mathbf{n}) \int_{-\infty}^{\infty} \frac{H_1 - 1}{H_1^{q-1}} dz = -(J_q \cdot \mathbf{n}) \int_{-\infty}^{\infty} \frac{H_1 - 1}{H_1^q} dz - \frac{\partial h_2}{\partial r}(R,\theta) - Q. \tag{4.36}$$

Here $(J_q \cdot \mathbf{n}) = -(J_q \cdot \hat{\mathbf{z}})(z = -\infty)$ is the flux matched to region III.

The expansion in region I is $h = h_0 + \epsilon h_1 + \epsilon^2 h_2 + o(\epsilon^2)$, which means h_2 solves

$$\nabla \cdot (h_0^q \nabla \Delta h_2) = 0. \tag{4.37}$$

This is the homogeneous version of (4.29), and therefore the relevant solvability conditions (for each coordinate direction) are the same as (4.33) with the left-hand side suppressed:

$$\int_{\partial D} x \nabla h_2 \cdot \mathbf{n} ds = 0 = \int_{\partial D} y \nabla h_2 \cdot \mathbf{n} ds. \tag{4.38}$$

We can now multiply (4.36) by x or y and integrate over ∂D and use (4.38). Again the Q term drops away and we are left with

$$X_t = -\frac{1}{\pi}\frac{\int_{-\infty}^{\infty}[H_1^{1-q} - H_1^{-q}]dz'}{R\int_{-\infty}^{\infty}[H_1^{2-q} - H_1^{1-q}]dz'}\left(\int_{\partial D}\mathbf{n}J_q\cdot\mathbf{n}ds\right). \tag{4.39}$$

4.4. Case $q = 2$. This case is similar to $q \in (2,3)$, but there are logarithmically diverging terms that require care. The flux of order ϵ^2 in region II satisfies the linear equation

$$\begin{aligned} 0 = (J_2\cdot\hat{\mathbf{z}})_z = \Bigg(H_1^2\Bigg[&(H_3)_{zz} - R^{-1}(H_2)_z - zR^{-2}(H_1)_z \\ &+ \frac{1}{2}U'''(H_1)H_2^2 + U''(H_1)H_3\Bigg]_z\Bigg)_z, \end{aligned} \tag{4.40}$$

which again says that the normal component of the flux is constant. The relevant solvability condition uses the function

$$\Phi = \int_{-\infty}^{z}\frac{H_1 - 1}{H_1^2}dz', \tag{4.41}$$

which diverges logarithmically:

$$\Phi = \ln(z) + O(1), \quad z\to\infty. \tag{4.42}$$

Multiplying Φ by (4.40) and integrating from $-\infty$ to some finite value $z = Z$ (since the result is unbounded as $Z\to\infty$) gives a result similar to (4.25):

(4.43)

$$0 = \Big[(J_2\cdot\hat{\mathbf{z}})\,\Phi - (H_1-1)[(H_3)_{zz} - U''(H_1)H_3] + (H_1)_z(H_3)_z - (H_1)_{zz}(H_3)\Big]_{-\infty}^{Z} + Q,$$

$$Q = \int_{-\infty}^{Z}(H_1-1)\left[R^{-1}(H_2)_z + zR^{-2}(H_1)_z + \frac{1}{2}U'''(H_1)H_2^2\right]_z dz.$$

Since the flux J_2 is nonzero, integrating (4.40) directly gives $(H_3)_{zzz}\sim 1/z^2$ for large z. Therefore H_3 is bounded and $(H_3)_z$ diverges logarithmically as $z\to+\infty$. The balance of logarithmically diverging terms in (4.43) gives

$$(H_3)_z = (J_2\cdot\mathbf{n})\ln(z) + O(1), \quad z\to\infty, \tag{4.44}$$

where $(J_q\cdot\mathbf{n}) = -(J_q\cdot\hat{\mathbf{z}})(z=-\infty)$ is the flux matched to region III.

In region I, we expand $h = h_0(x,t) + \epsilon h_1 + \epsilon^2\ln(1/\epsilon)h_* + o(\epsilon^2\ln(1/\epsilon))$. Then h_* solves the linear equation (4.1), and the solvability arguments proceed as before. Like the case $q\in(2,3)$, $R_t = 0$ to leading order (albeit mass exchange is only logarithmically slower). The other solvability conditions are obtained by taking inner products with ψ_x, ψ_y, which produces a result analogous to (4.33):

$$X_t\cdot\hat{\mathbf{x}}\int_D \psi_x(h_0)_x\,d\mathbf{x} = -\int_{\partial D} x\nabla h_*\cdot\mathbf{n}ds. \tag{4.45}$$

Matching conditions that relate $(h_*)_x$ to $(H_3)_z$ are now derived. It is assumed that region I and II solutions describe the same solution on some overlapping region

$1 \ll z \ll [\epsilon \ln(1/\epsilon)]^{-1}$. Within this region, a Taylor expansion is justified for h_0, h_1 but not h_* so that

$$\begin{aligned}
&(H_1)_z + \epsilon(H_2)_z + \epsilon^2(H_3)_z + o(\epsilon^2) \\
&= -(h_0)_r - \epsilon(h_1)_r - \epsilon^2 \ln(1/\epsilon)(h_*)_r + o(\epsilon^2 \ln(1/\epsilon)) \\
&= -(h_0)_r(R,\theta) - \epsilon\Big[(h_1)_r(R,\theta) + (h_0)_{rr}(R,\theta)z\Big] \\
&\quad - \epsilon^2 \ln(1/\epsilon)(h_*)_r(R,\theta) + o(\epsilon^2 \ln(1/\epsilon)).
\end{aligned} \tag{4.46}$$

Equating terms at order 1 and ϵ gives the usual matching conditions for regular expansions. For the logarithmic terms, the procedure is to take $\epsilon \to 0$ and $z \sim [\epsilon \ln(1/\epsilon)]^{-1}$ simultaneously. Using (4.44), for large z we have

$$(H_3)_z = (J_2 \cdot \mathbf{n}) \ln\Big([\epsilon \ln(1/\epsilon)]^{-1}\Big) + O(1) = (J_2 \cdot \mathbf{n}) \ln(1/\epsilon) + \mathcal{O}\Big(\ln(\ln(1/\epsilon))\Big). \tag{4.47}$$

Inserting into (4.46) and equating terms of order $\epsilon^2 \ln(1/\epsilon)$ gives

$$(J_2 \cdot \mathbf{n}) = -(h_*)_r(R,\theta). \tag{4.48}$$

This can be combined with (4.45) to yield

$$X_t = -\frac{1}{\pi} \frac{R^2}{\int_0^R \Psi(r) r^2 dr} \left(\int_{\partial D} \mathbf{n} J_q \cdot \mathbf{n}\, ds \right). \tag{4.49}$$

4.5. Case $q = 3$. This case is similar to both $q > 3$ and $q \in (2,3)$, but there are again logarithmically diverging terms. The flux of order ϵ^3 in region II satisfies the linear equation

$$\begin{aligned}
0 = (J_3 \cdot \hat{\mathbf{z}})_z = \Bigg(H_1^3 \Big[&(H_3)_{zz} - R^{-1}(H_2)_z - zR^{-2}(H_1)_z \\
&+ \frac{1}{2} U'''(H_1) H_2^2 + U''(H_1) H_3 \Big]_z \Bigg)_z .
\end{aligned} \tag{4.50}$$

A solvability argument identical to the case $q \in (2,3)$ produces

$$(J_3 \cdot \mathbf{n}) \int_{-\infty}^{\infty} \frac{H_1 - 1}{H_1^3} dz' = (H_3)_z - Q. \tag{4.51}$$

In region I, we expand $h = h_0(x,t) + \epsilon h_1 + \epsilon^2/\ln(1/\epsilon) h_* + o(\epsilon^2/\ln(1/\epsilon))$, so that h_* solves the linear equation (4.1) with $q = 3$, and the solvability arguments proceed as before. As for all cases $q \geq 2$, $R_t = 0$ to leading order. In this case, the inner products with ψ_x, ψ_y diverge logarithmically, so we integrate on a disk $D(\rho)$ with radius $\rho < R$ and consider the asymptotics as $\rho \to R$. Multiplying by ψ_x and integrating gives

$$\begin{aligned}
(X_t \cdot \hat{\mathbf{x}}) \int_{D(\rho)} \psi_x (h_0)_x \, d\mathbf{x} &= \int_{\partial D(\rho)} \psi_x h_0^3 \nabla \Delta h_* \cdot \mathbf{n} ds - \int_{\partial D(\rho)} h_0^3 (\Delta h_*) \nabla \psi_x \cdot \mathbf{n} ds \\
&\quad - \int_{\partial D(\rho)} x \nabla h_* \cdot \mathbf{n} ds + \int_{\partial D(\rho)} h_* \cos\theta \, ds = B_1 + B_2 + B_3 + B_4.
\end{aligned} \tag{4.52}$$

The integral on the left-hand side has a logarithmic singularity as $\rho \to R$ because of (4.9); in particular,

$$\int_{D(\rho)} \psi_x (h_0)_x \, d\mathbf{x} = -\pi R^2 \ln|R-\rho| + \mathcal{O}(1), \quad \rho \to R. \tag{4.53}$$

Matching conditions (which are detailed below) require $\nabla h_* \sim C \ln|R-r|$. As a consequence, we find that h_* is bounded and

$$\nabla \Delta h_* \sim |R-r|^{-2}, \quad \Delta h_* \sim |R-r|^{-1} \tag{4.54}$$

as $r \to R$. All this implies that the integrals B_1, B_2, B_4 are bounded as $\rho \to R$ but B_3 diverges logarithmically. Using (4.52)–(4.53) gives

$$\int_{\partial D(\rho)} x \nabla h_* \cdot \mathbf{n} ds = \pi R^2 (X_t \cdot \hat{\mathbf{x}}) \ln|R-\rho| + \mathcal{O}(1), \quad \rho \to R. \tag{4.55}$$

The matching condition that relates $(h_*)_r$ to $(H_3)_z$ is derived as for $q = 2$. Equating expansions for h_r in regions I and II, then for $1 \ll z \ll \log(1/\epsilon)$,

$$\begin{aligned} &(H_1)_z + \epsilon (H_2)_z + \epsilon^2 (H_3)_z + o(\epsilon^2) \\ &= -(h_0)_r - \epsilon (h_1)_r - \epsilon^2 / \ln(1/\epsilon)(h_*)_r + o(\epsilon^2/\ln(1/\epsilon)) \\ &= -(h_0)_r(R,\theta) - \epsilon \Big[(h_1)_r(R,\theta) + (h_0)_{rr}(R,\theta) z \Big] \\ &\quad - \epsilon^2 (h_1)_{rr}(R,\theta) z - \epsilon^2 / \ln(1/\epsilon)(h_*)_r + o(\epsilon^2/\ln(1/\epsilon)). \end{aligned} \tag{4.56}$$

Let $(h_*)_r \sim C \ln|R-r|$, $r \to R$, where C is to be determined. Taking $\epsilon \to 0$ with $z \sim \ln(1/\epsilon)$ simultaneously implies for large z

$$(h_*)_r = C \ln(\epsilon z) + \mathcal{O}(1) = C \ln(\epsilon) + \mathcal{O}(\ln(\ln(1/\epsilon))), \quad \epsilon \to 0. \tag{4.57}$$

Inserting into (4.56) and equating terms of order ϵ^2, we obtain

$$C = \lim_{z \to \infty} -(H_3)_z. \tag{4.58}$$

Finally, combining (4.51), (4.55), (4.58),

$$X_t = -\frac{1}{\pi} \frac{\int_{-\infty}^{\infty} [H_1^{-2} - H_1^{-3}] dz}{R} \left(\int_{\partial D} \mathbf{n} J_q \cdot \mathbf{n} \, ds \right). \tag{4.59}$$

5. Effective medium approximation and identification of timescales. One potentially useful approximation to the free boundary problem described in section 2 utilizes Green's functions similar to the effective medium approximations for standard Ostwald ripening [38]. This is employed to determine timescales and study large systems of interacting droplets.

5.1. Reduced system. Let X_k, R_k, $k = 1, \ldots, N$, be the droplet centers and radii. We want to solve $\Delta P = 0$ exterior to the droplets, i.e., for all $\mathbf{x}$, $|\mathbf{x} - X_k| > R_k$, subject to the boundary conditions

$$P(\mathbf{x}) = \frac{2}{R_k}, \quad |\mathbf{x} - X_k| = R_k. \tag{5.1}$$

The simplest approximation looks for a solution as a sum of Green's functions,

$$P(\mathbf{x}) = B_0 + \sum_{k=1}^{N} B_k \ln|\mathbf{x} - X_k|^2. \tag{5.2}$$

For each $j = 1, \ldots, N$, the boundary condition which one wishes to satisfy is

$$\frac{2}{R_j} = B_0 + \sum_{k=1}^{N} B_k \ln|\mathbf{x} - X_k|^2 \quad \text{for} \quad |\mathbf{x} - X_j| = R_j. \tag{5.3}$$

Assuming the droplets are well separated, the approximation $|\mathbf{x} - X_k| \approx |X_j - X_k|$ holds on the boundary of droplet $j \neq k$, giving

$$\frac{2}{R_j} = B_0 + B_j \ln(R_j^2) + \sum_{k \neq j} B_k \ln|X_j - X_k|^2, \quad j = 1, \ldots, N. \tag{5.4}$$

The system is completed by the requirement that there be no flux at infinity:

$$\int_S \nabla P \cdot n \to 0, \tag{5.5}$$

as the curve S (take it to be a giant circle) is taken out to infinity. As $\mathbf{x} \to \infty$, $1/|\mathbf{x} - R_k| \approx 1/|\mathbf{x}|$, and therefore

$$\int_S \nabla P \cdot n \to \sum_{k=1}^{N} B_k \left(\int_S \frac{1}{|\mathbf{x}|} ds \right) = 2\pi \sum_{k=1}^{N} B_k. \tag{5.6}$$

This integral will be zero only if

$$\sum_{k=1}^{N} B_k = 0. \tag{5.7}$$

Equations (5.4) and (5.7) define an $(N+1) \times (N+1)$ linear problem to be solved.

The integral in (2.5) to be computed for each j is

$$\int_{\partial D_j} J \cdot \mathbf{n}\, ds = -\int_{\partial D_j} \nabla P \cdot \mathbf{n}\, ds = 4\pi B_j. \tag{5.8}$$

The integral in (2.6) to be evaluated for each j is

$$\begin{aligned} \int_{\partial D_j} (J \cdot \mathbf{n})\mathbf{n}\, ds &= -\int_{\partial D_j} \left(\sum_k B_k \frac{2(\mathbf{x} - X_k) \cdot \mathbf{n}}{|\mathbf{x} - X_k|^2} \right) ds(\mathbf{x}) \\ &\approx -2 \left(\sum_{k \neq j} B_k \frac{X_j - X_k}{|X_j - X_k|^2} \right) \cdot \left(\int_{\partial D_j} \mathbf{n} \otimes \mathbf{n}\, ds \right), \end{aligned} \tag{5.9}$$

where the same approximation $|\mathbf{x} - X_k| \approx |X_j - X_k|$ as before was used. Since

$$\int_{\partial D_j} \mathbf{n} \otimes \mathbf{n}\, ds = \pi R_j \mathbf{I}, \tag{5.10}$$

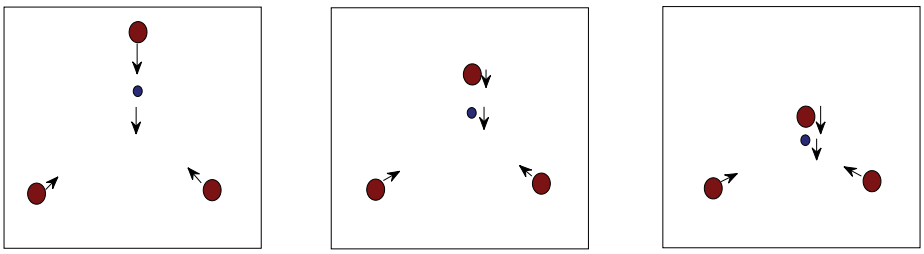

FIG. 5.1. *Example numerical solution of an approximate system with four initial droplets. The net repulsion experienced by the drop in the center is small, allowing one of the large droplets to catch up.*

where $\mathbf{I}$ is the identity matrix, it follows that

$$\int_{\partial D_j} (J \cdot \mathbf{n})\mathbf{n}\, ds \approx -2\pi R_j \sum_{k \neq j} B_k \frac{X_j - X_k}{|X_j - X_k|^2}. \tag{5.11}$$

It is instructive to examine a simple situation where only two droplets interact. By virtue of the quasi-steady diffusion (2.4) it follows that the flux J will on average be toward the smaller drop. In the context of the above approximation, that means that if $R_1 > R_2$, then $B_1 > 0 > B_2$. Using (2.6) and (5.11), it follows that the velocity of both droplets is in the direction of the *smaller* droplet.

By virtue of the mobility factor (2.7), a smaller droplet moves faster, and therefore it would simply "run away" from a single large droplet. On the other hand, if a smaller droplet is surrounded by several large droplets, the net repulsion can be small enough so that merging with a larger droplet is possible. Figure 5.1 shows a numerically computed example with three large droplets and a small droplet, which eventually touches one of the larger droplets. Simulations of the thin film equation indicate that this initiates a rapid coalescence of both drops [29].

5.2. Dynamic timescales. Consider now a reasonably large array of droplets which all have a similar size R and typical spacing L, so that the volume per unit area is

$$H_{average} = \frac{R^3}{L^2}, \tag{5.12}$$

which is constant as time progresses.

Timescale for ripening. The approximation (5.2) gives the scaling

$$B_j \sim R^{-1}/\ln L, \tag{5.13}$$

which with (5.8) further implies

$$\int_{\partial D_j} J \cdot \mathbf{n}\, ds \sim R^{-1}/\ln L. \tag{5.14}$$

For exponents $q < 2$, using (2.5), the timescale for ripening (i.e., mass exchange) can be computed as

$$\tau_{ripe} \sim \frac{R}{R_t} \sim R^4 \ln L \sim H_{average}^{4/3} L^{8/3} \ln L, \quad q < 2. \tag{5.15}$$

For exponents $q \geq 2$, the ripening dynamics occur on a timescale of the flux, i.e., ϵ^q rather than $\tau(\epsilon)$. This can be accommodated by including an extra factor in the timescale:

$$\tau_{ripe} \sim \frac{R}{R_t} \sim \frac{\tau(\epsilon)}{\epsilon^q} H_{average}^{4/3} L^{8/3} \ln L, \quad q \geq 2. \tag{5.16}$$

Timescale for migration. Using (5.11) and (5.13), one can obtain

$$\int_{\partial D_j} (J \cdot \mathbf{n})\mathbf{n}\, ds \sim L^{-1}/\ln L. \tag{5.17}$$

Using (2.6), the timescale for migration can be computed as

$$\tau_{mig} \sim \frac{L}{X_t} \sim \begin{cases} H_{average}^{2/3} L^{10/3} \ln L, & q < 2, \\ H_{average}^{\frac{4-q}{3}} L^{(14-2q)/3} \ln L, & q \in [2,3], \\ H_{average}^{1/3} L^{8/3} \ln L, & q > 3. \end{cases} \tag{5.18}$$

The limit of large droplet size in the unscaled equation. Here we show that our scaling results are, suitably interpreted, the same as those derived in the companion paper [9]. The starting point there was the unscaled thin film equation

$$h_t = \nabla \cdot (h^q \nabla p), \quad p = U'(h) - \Delta h, \quad q > 0. \tag{5.19}$$

In [9], the limit of large droplet volume was considered, in contrast to a small precursor film. In this case, let $V \gg 1$ be a typical droplet volume with characteristic interdroplet distance L'. This suggests that the natural small parameter is $\epsilon = V^{-1/3}$. Rescaling (5.19) using

$$x \to \epsilon^{-1} x, \quad t \to \tau(\epsilon)^{-1} \epsilon^{q-4}, \quad h \to h\epsilon^{-1} \tag{5.20}$$

gives exactly (1.1). The average droplet size after rescaling is $R = 1$, and the characteristic distance between droplets is

$$L = \epsilon L' = \frac{V^{1/6}}{\overline{H}^{1/2}}, \tag{5.21}$$

where $\overline{H} = V/(L')^2$. The mass density for the scaled equation is

$$H_{average} = \frac{1}{\epsilon^2 (L')^2} = \frac{\overline{H}}{V^{1/3}}. \tag{5.22}$$

Timescales with respect to the unscaled equation (5.19) can now be written in terms of V and $\overline{H}$. For the ripening times given by either (5.15) or (5.16) one obtains

$$\tau_{ripe}^{unscaled} = \tau(\epsilon)\epsilon^{4-q}\tau_{ripe} \sim V^{4/3} \ln V + \mathcal{O}(1), \quad V \to \infty. \tag{5.23}$$

For the migration timescale (5.18) one has

$$\tau_{mig}^{unscaled} = \tau(\epsilon)\epsilon^{4-q}\tau_{mig} = \mathcal{O}(1) + \frac{1}{\overline{H}} \begin{cases} V^{5/3} \ln V, & q \in (0,2), \\ V^{5/3}, & q = 2, \\ V^{\frac{7-q}{3}} \ln V, & q \in (2,3), \\ V^{4/3} \ln^2 V, & q = 3, \\ V^{4/3} \ln V, & q > 3. \end{cases} \quad V \to \infty, \tag{5.24}$$

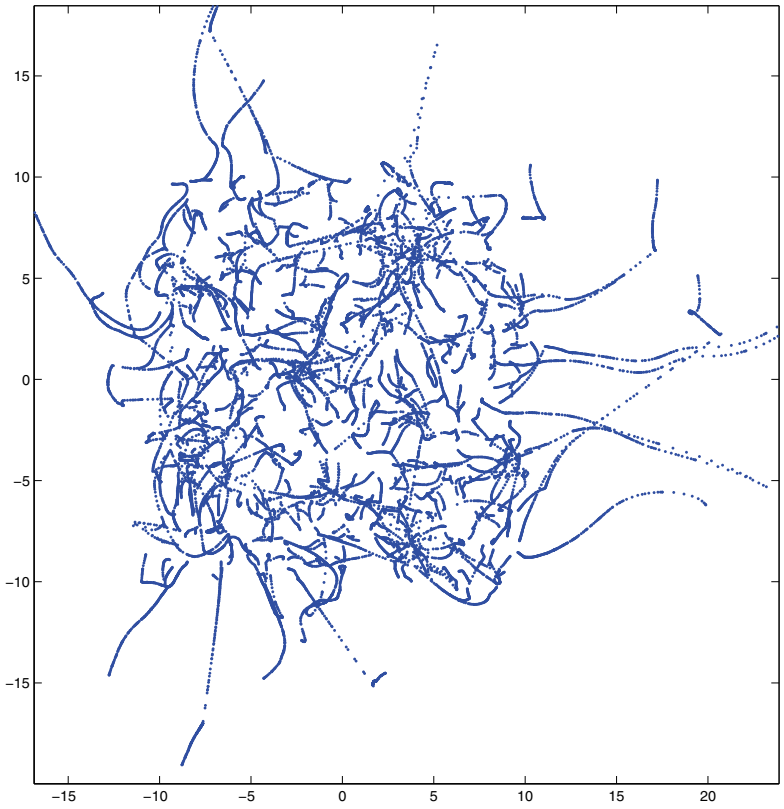

FIG. 6.1. *Trajectories for a simulation with* 500 *initial droplets* ($q = 3$). *The direction of motion is mostly outward from the center. Note that small, uncoalesced droplets on the fringes are repelled.*

6. Large scale coarsening by coalescence. We conclude by using the approximations of the previous section to study the evolution of a large assembly of droplets. We focus on the most relevant mobility exponent $q = 3$, which corresponds to a fluid with Newtonian viscosity and a no-slip boundary condition. In doing this, the exchange of material between droplets is ignored, and only the leading order effect, migration, is considered. There are no boundaries in the calculation, so that (5.5) applies. An ad hoc criterion for coalescence is applied, which states that when the perimeters of two droplets overlap, their volume is combined and the center of mass is preserved.

Figure 6.1 is an illustration of the dynamics. The simulation was started with 500 droplets in random locations, each with a random but nearly uniform radius. Droplets in the middle of the assembly coalesce first, simply because they have a greater number of neighbors. As time progresses, it follows that smaller, more mobile droplets on the fringes will be driven away, since the motion is opposite the flux, which is toward larger droplets. The amount of time that droplets take to move (relative to the interdroplet distance) increases since the driving force given by flux decreases with increasing droplet size.

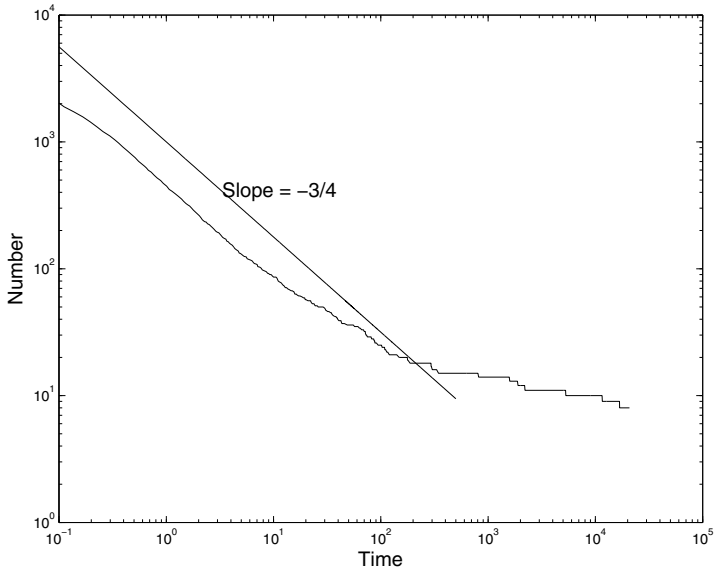

FIG. 6.2. *Dynamic scaling of coalescence-driven coarsening ($q = 3$), using* 5000 *initial droplets. A line with slope* $-3/4$ *is provided for comparison to the predictions of* [29].

Figure 6.2 shows the droplet number plotted as a function of time, for a simulation with 5000 droplets initially. Dynamic scaling of the coarsening process was predicted [29]; in particular, the relevant length scale (the typical interdroplet distance L) should increase as $t^{3/8}$. Since the number of droplets N scales according to

$$NL^2 \sim \text{area of domain},$$

N should scale in time like $t^{-3/4}$. This is more or less borne out by the results in Figure 6.2. At late times when the array has spread out to a somewhat larger area, there is a slowing of the coarsening process, also seen in the computational results.

7. Conclusions. The main outcome of this paper is to establish a concrete link between a class of thin film equations and a free boundary problem for the motion of the contact line interface. In contrast to the classical situation of Ostwald ripening, we have shown that migration of droplets, and ultimately coalescence, is a likely mechanism for coarsening. Another feature which distinguishes this problem is its mixed dimensionality: droplets are three-dimensional, but the quasi-steady diffusion of material between them is effectively two-dimensional. This leads to dynamic scaling with exponents different than the familiar "1/3" power law.

There is some experimental support for the conclusions which we reach. Limary and Green [15, 16] examined the late stage structural evolution of droplets and measured their size and shape distributions. They found that droplet size (measured as a length scale) evolved as a power law with an exponent that varied from 1/10 to about 2/5. They conclude from their observations that "coarsening occurs via a self-similar, dynamic coalescence process, not Ostwald ripening" (referring to the exchange of material).

As mentioned in the introduction, [32] derives dynamic equations for droplet radius and position in the same thin film model as ours for mobility exponent $q = 3$. The procedure used there does not involve systematic asymptotic expansions and solvabil-

ity conditions, but rather poses a traveling wave problem that loosely derives from the thin film equation. The authors connect the traveling wave speed to the influence felt by the disjoining pressure at the foot of the droplet. The resulting formulas are vaguely similar to ours but are not quantitatively the same. Most significantly, their assessment of the sign of migration seems to be opposite of ours and contradicts other analytical results [9, 11, 12] as well as direct numerical simulation of the partial differential equation [11, 29]. Indeed, in section IV.B of their paper, they claim that in a two-droplet system "both droplets migrate in the direction of the larger droplet" and show calculations where smaller droplets are attracted to larger droplets. According to (2.6), a larger droplet would move toward a smaller droplet since motion is *opposite* of the flux J. This certainly calls into question the reasoning that leads to their formulation.

There is reason to believe that our results (or at least our analytical procedures) are relevant for a variety of related thin film problems. The main ingredients which we required were the formation of near-equilibrium structures (droplets) and a separation of timescales between their formation and interaction. This separation of timescales is a simple consequence of the nearly degenerate kinetics common to many thin film models. A variety of other phenomena can create instability leading to structure formation and interaction. For example, the Rayleigh–Taylor or Rayleigh–Plateau instabilities lead to formation of migrating liquid ridges [10, 17]. Migration effects similar to ours have also been reported for droplets subject to Marangoni effects [4], chemically driven droplets [31], and two-layer fluids [18]. More broadly, one might expect that degenerate diffusion in other phase separation processes can lead to alternative mechanisms to coarsening.

Acknowledgments. The author is grateful for discussions with Felix Otto, Tobias Rump, and Dejan Slepčev, and for the hospitality afforded during his visit to the University of Bonn.

REFERENCES

[1] J. Becker, G. Grün, R. Seemann, H. Mantz, K. Jacobs, K. R. Mecke, and R. Blossey, *Complex dewetting scenarios captured by thin-film models*, Nature Materials, 2 (2003), pp. 59–62.

[2] A. L. Bertozzi, G. Grün, and T. P. Witelski, *Dewetting films: Bifurcations and concentrations*, Nonlinearity, 14 (2001), pp. 1569–1592.

[3] M. Bestehorn and K. Neuffer, *Surface patterns of laterally extended thin liquid films in three dimensions*, Phys. Rev. Lett., 87 (2001), paper 046101.

[4] M. Bestehorn, A. Pototsky, and U. Thiele, *3D large scale Marangoni convection in liquid films*, European Phys. J. B Condens. Matter Phys., 33 (2003), pp. 457–467.

[5] J. W. Cahn and J. E. Hilliard, *Free energy of a nonuniform system* I: *Interfacial free energy*, J. Chem. Phys., 28 (1957), pp. 258–267.

[6] P. Constantin, T. F. Dupont, R. E. Goldstein, L. P. Kadanoff, M. J. Shelley, and S.-M. Zhou, *Droplet breakup in a model of the Hele-Shaw cell*, Phys. Rev. E, 47 (1993), pp. 4169–4181.

[7] P. G. de Gennes, *Wetting: Statics and dynamics*, Rev. Mod. Phys., 57 (1985), pp. 827–880.

[8] R. Fetzer, K. Jacobs, A. Münch, B. Wagner, and T. P. Witelski, *New slip regimes and the shape of dewetting thin liquid films*, Phys. Rev. Lett., 95 (2005), paper 127801.

[9] K. Glasner, F. Otto, T. Rump, and D. Slepčev, *Ostwald ripening of droplets: The role of migration*, European J. Appl. Math., (2008), to appear.

[10] K. B. Glasner, *The dynamics of pendant droplets on a one-dimensional surface*, Phys. Fluids, 19 (2007), paper 102104.

[11] K. B. Glasner and T. P. Witelski, *Coarsening dynamics of dewetting films*, Phys. Rev. E, 67 (2003), paper 016302.

[12] K. B. Glasner and T. P. Witelski, *Collision versus collapse of droplets in coarsening of dewetting thin films*, Phys. D, 209 (2005), pp. 80–104.

[13] S. Kalliadasis and U. Thiele, eds., *Thin Films of Soft Matter*, Springer, Wien, New York, 2007.
[14] I. M. Lifshitz and V. V. Slyozov, *The kinetics of precipitation from supersaturated solid solutions*, J. Chem. Phys. Solids, 19 (1961), pp. 35–50.
[15] R. Limary and P. F. Green, *Late-stage coarsening of an unstable structured liquid film*, Phys. Rev. E, 66 (2002), paper 021601.
[16] R. Limary and P. F. Green, *Dynamics of droplets on the surface of a structured fluid film: Late-stage coarsening*, Langmuir, 19 (2003), pp. 2419–2424.
[17] J. R. Lister, J. M. Rallison, A. A. King, L. J. Cummings, and O. E. Jensen, *Capillary drainage of an annular film: The dynamics of collars and lobes*, J. Fluid Mech., 552 (2006), pp. 311–343.
[18] D. Merkt, A. Pototsky, M. Bestehorn, and U. Thiele, *Long-wave theory of bounded two-layer films with a free liquid-liquid interface: Short- and long-time evolution*, Phys. Fluids, 17 (2005), paper 064104.
[19] V. S. Mitlin, *Dewetting of a solid surface: Analogy with spinodal decomposition*, J. Coll. Int. Sci., 156 (1993), pp. 491–497.
[20] V. S. Mitlin, *Dewetting revisited: New asymptotics of the film stability diagram and the metastable regime of nucleation and growth of dry zones*, J. Coll. Int. Sci., 227 (2000), pp. 371–379.
[21] V. S. Mitlin, *Numerical study of a Lifshitz-Slyozov-like metastable dewetting model*, J. Coll. Int. Sci., 233 (2001), pp. 153–158.
[22] V. S. Mitlin and N. V. Petviashvili, *Nonlinear dynamics of dewetting: Kinetically stable structures*, Phys. Lett. A, 192 (1994), pp. 323–326.
[23] A. Münch, B. Wagner, and T. Witelski, *Lubrication models with small to large slip lengths*, J. Engrg. Math., 53 (2005), pp. 359–383.
[24] B. Niethammer and F. Otto, *Domain coarsening in thin films*, Comm. Pure Appl. Math., 54 (2001), pp. 361–384.
[25] B. Niethammer and R. L. Pego, *On the initial-value problem in the Lifshitz–Slyozov–Wagner theory of Ostwald ripening*, SIAM J. Math. Anal., 31 (2000), pp. 467–485.
[26] L. Onsager, *Reciprocal relations in irreversible processes.* ii., Phys. Rev., 38 (1931), pp. 2265–2279.
[27] A. Oron, *Three-dimensional nonlinear dynamics of thin liquid films*, Phys. Rev. Lett., 85 (2000), pp. 2108–2111.
[28] A. Oron, S. H. Davis, and S. G. Bankoff, *Long-scale evolution of thin liquid films*, Rev. Mod. Phys., 69 (1997), pp. 931–980.
[29] F. Otto, T. Rump, and D. Slepčev, *Coarsening rates for a droplet model: Rigorous upper bounds*, SIAM J. Math. Anal., 38 (2006), pp. 503–529.
[30] R. L. Pego, *Front migration in the nonlinear Cahn-Hilliard equation*, Proc. R. Soc. Lond. A, 422 (1989), pp. 261–278.
[31] L. M. Pismen, *Perturbation theory for traveling droplets*, Phys. Rev. E (3), 74 (2006), paper 041605.
[32] L. M. Pismen and Y. Pomeau, *Mobility and interactions of weakly nonwetting droplets*, Phys. Fluids, 16 (2004), pp. 2604–2612.
[33] G. Reiter, *Dewetting of thin polymer films*, Phys. Rev. Lett., 68 (1992), pp. 75–78.
[34] R. Seemann, S. Herminghaus, C. Neto, S. Schlagowski, D. Podzimek, R. Konrad, H. Mantz, and K. Jacobs, *Dynamics and structure formation in thin polymer melt films*, J. Phys. Condensed Matter, 17 (2005), pp. 267–290.
[35] R. A. Segalman and P. F. Green, *Dynamics of rims and the onset of spinodal dewetting at liquid/ liquid interfaces*, Macromolecules, 32 (1999), pp. 801–807.
[36] A. Sharma and R. Khanna, *Pattern formation in unstable thin liquid films*, Phys. Rev. Lett., 81 (1998), pp. 3463–3466.
[37] U. Thiele, M. G. Velarde, and K. Neuffer, *Dewetting: Film rupture by nucleation in the spinodal regime*, Phys. Rev. Lett., 87 (2001), paper 016104.
[38] P. W. Voorhees, *The theory of Ostwald ripening*, J. Statist. Phys., 38 (1985), pp. 231–252.
[39] C. Wagner, *Theorie for alterung von niederschlagen durch umlosen*, Z. Elektrochemie, 65 (1961), pp. 581–594.
[40] S. J. Watson, F. Otto, B. Y. Rubinstein, and S. H. Davis, *Coarsening dynamics of the convective Cahn-Hilliard equation*, Phys. D, 178 (2003), pp. 127–148.
[41] D. E. Weidner and L. W. Schwartz, *Contact-line motion of shear-thinning liquids*, Phys. Fluids, 6 (1994), pp. 3535–3538.
[42] R. Xie, A. Karim, J. F. Douglas, C. C. Han, and R. A. Weiss, *Spinodal dewetting of thin polymer films*, Phys. Rev. Lett., 81 (1998), pp. 1251–1254.